Accepted Author Manuscript
NOTICE: This is the author's version of a work that was accepted for publication in *The Journal of Physiology (London)*. Changes resulting from the publishing process, such as peer review, editing, corrections, structural formatting, and other quality control mechanisms may not be reflected in this document. Changes may have been made to this work since it was submitted for publication. A definitive version was subsequently published in *J Physiol*, 2016, 594:2537–2553.

DOI: 10.1113/JP271573

Stochastic pacing reveals the propensity to cardiac action potential alternans and uncovers its underlying dynamics

Yann Prudat,[1] Roshni V. Madhvani,[2] Marina Angelini,[2] Nils P. Borgstom,[3] Alan Garfinkel,[4] Hrayr S. Karagueuzian,[4] James N. Weiss,[4,5,6] Enno de Lange,[7] Riccardo Olcese,[2,4,5] and Jan P. Kucera[1]

[1]Dept. of Physiology, University of Bern, Bern, Switzerland

[2]Dept. of Anesthesiology and Perioperative Medicine, Division of Molecular Medicine, David Geffen School of Medicine, University of California, Los Angeles, USA

[3]Dept. of Bioengineering, University of California, Los Angeles, USA

[4]Cardiovascular Research Laboratory, David Geffen School of Medicine, University of California, Los Angeles, USA

[5]Dept. of Physiology, David Geffen School of Medicine, University of California, Los Angeles, USA

[6]Dept. of Medicine (Cardiology), David Geffen School of Medicine, University of California, Los Angeles, USA

[7]Dept. of Knowledge Engineering, Maastricht University, Maastricht, The Netherlands

Running title: Investigating alternans by stochastic pacing

Keywords: cardiac action potential; alternans; restitution; stochastic pacing; ventricular myocytes; ryanodine

Corresponding author:

Jan P. Kucera

Department of Physiology, University of Bern, Bühlplatz 5, 3012 Bern, Switzerland

E-mail: kucera@pyl.unibe.ch

Table of Contents category: Cardiovascular

source: https://doi.org/10.7892/boris.92663 | downloaded: 25.4.2024

Key points

- Beat-to-beat alternation (alternans) of the cardiac action potential duration is known to precipitate life-threatening arrhythmias. Alternans can be driven by the kinetics of voltage-gated membrane currents or by instabilities in intracellular calcium fluxes.

- To prevent alternans and associated arrhythmias, suitable markers must be developed to quantify the susceptibility to alternans. Previous theoretical studies showed that the eigenvalue of the alternating eigenmode represents an ideal marker of alternans.

- Using rabbit ventricular myocytes, we show that this eigenvalue can be estimated in practice by pacing these cells at intervals varying stochastically.

- We also show that stochastic pacing permits the estimation of further markers distinguishing between voltage-driven and calcium-driven alternans.

- Our study opens the perspective to use stochastic pacing during clinical investigations and in patients with implanted pacing devices to determine the susceptibility to, and the type of alternans, which are both important to guide preventive or therapeutic measures.

Abstract

Alternans of the cardiac action potential (AP) duration (APD) is a well-known arrhythmogenic mechanism. APD depends on several preceding diastolic intervals (DIs) and APDs, which complicates the prediction of alternans. Previous theoretical studies pinpointed a marker called λ_{alt} that directly quantifies how an alternating perturbation persists over successive APs. When the propensity to alternans increases, λ_{alt} decreases from 0 to –1. Our aim was to quantify λ_{alt} experimentally using stochastic pacing and to examine whether stochastic pacing allows discriminating between voltage-driven and Ca^{2+}-driven alternans. APs were recorded in rabbit ventricular myocytes paced at cycle lengths (CLs) decreasing progressively and incorporating stochastic variations. Fitting APD with a function of two previous APDs and CLs permitted to estimate λ_{alt} along with additional markers characterizing whether the dependence of APD on previous DIs or CLs is strong (typical for voltage-driven alternans) or weak (Ca^{2+}-driven alternans). During the recordings, λ_{alt} gradually decreased from around 0 towards –1. Intermittent alternans appeared when λ_{alt} reached –0.8 and was followed by sustained alternans. The additional markers detected that alternans was Ca^{2+}-driven in control experiments and voltage-driven in the presence of ryanodine. This distinction could be made even before alternans was manifest (specificity/sensitivity >80% for $-0.4>\lambda_{alt}>-0.5$). These observations were confirmed in a mathematical model of a rabbit ventricular myocyte. In conclusion, stochastic pacing allows the practical estimation of λ_{alt} to reveal the onset of alternans and distinguishes between voltage-driven and Ca^{2+}-driven mechanisms, which is important since these two mechanisms may precipitate arrhythmias in different manners.

Abbreviations. AP, action potential; APD, action potential duration; AR model: autoregressive model; ARMA model: autoregressive-moving-average model; CL, cycle length; DI, diastolic interval; ORd, O'Hara-Virag-Varró-Rudy human ventricular cell model. λ_{alt}, alternans eigenvalue.

Introduction

Alternation of the cardiac action potential duration (APD) from beat to beat is a well-known arrhythmogenic mechanism. Alternans can lead to spatial dispersion of refractoriness potentiating conduction block, reentry and life-threatening arrhythmias such as atrial or ventricular fibrillation (Pastore *et al.* 1999; Weiss *et al.* 2006; Franz *et al.* 2012; Karagueuzian *et al.* 2013; Taggart *et al.* 2014; Verrier & Malik 2015; Wagner *et al.* 2015). Alternans can occur in a variety of forms and mechanisms (Qu *et al.* 2010; Edwards & Blatter 2014; Wagner *et al.* 2015). At the cellular level, alternans can result from the dependence of APD on the previous diastolic interval (DI), due to the amplitude and kinetics of voltage-gated ion currents (voltage-driven alternans) (Koller *et al.* 1998; Pastore *et al.* 1999). Alternans can also result from a dynamic instability in intracellular Ca^{2+} cycling, in particular due to the nonlinear behaviour of Ca^{2+}-induced Ca^{2+} release and the bidirectional interaction between APD and the Ca^{2+} transient (Ca^{2+}-driven alternans) (Qu *et al.* 2010; Edwards & Blatter 2014; Wagner *et al.* 2015). At the tissue and organ levels, alternans is modulated by intercellular interactions, conduction velocity restitution and pacing rate (Watanabe *et al.* 2001; Echebarria & Karma 2002). These multiscale mechanisms interact dynamically and give rise to complex spatiotemporal alternans patterns (Sato *et al.* 2006; Mironov *et al.* 2008; Gizzi *et al.* 2013).

In the initial theory of alternans (Nolasco & Dahlen 1968; Guevara *et al.* 1981; Chialvo *et al.* 1990), APD is described as a nonlinear function of the previous DI (restitution function). Alternans occurs as a bifurcation when the slope of this function becomes ≥ 1. Hence, the propensity to alternans is classically evaluated by determining APD restitution slopes using downsweep or S1S2 pacing protocols (Kalb *et al.* 2004; Tolkacheva *et al.* 2006).

Several studies suggest that this approach is not always appropriate and some provide arguments against it. For example, none of the conventional restitution slopes predicted alternans in bullfrog myocardium (Kalb *et al.* 2004), and the authors suggested that the memory of previous pacing cycles must in fact be taken into account. In rabbit hearts, it was shown that these slopes were statistically different from 1 at the onset of alternans

(Cram *et al.* 2011). Another study showed that during hypokalaemia, the predictive power of APD restitution in promoting alternans fails (Osadchii *et al.* 2010). Using a system permitting the real time control of the DI, further investigators (Wu & Patwardhan 2006) showed that in canine ventricle, alternans can occur even if the DI is kept constant from beat to beat. This demonstrates that APD does not depend only on the previous DI and that memory of previous pacing cycles must be considered.

Because APDs, DIs and cycle lengths (CLs) are intricately linked, a perturbation of one parameter will propagate from one beat to the next and influence the sequence of the others parameters over several cycles. To untangle these interactions, modern paradigms to evaluate alternans should therefore rely on multivariate analyses taking entire sequences of APDs, DIs and CLs into account. Intuitively, it would be a great advantage to have a marker that quantifies how a perturbation of one of these parameters is transmitted over subsequent cycles and how fast or how slow it decays. Theoretical studies (Li & Otani 2003; Otani *et al.* 2005) have shown that the activity of a cardiac cell can be decomposed into distinct eigenmodes, i.e., patterns that recur every beat after being scaled by specific numbers called eigenvalues (λ), producing the series 1, λ, λ^2, λ^3, … over successive beats, as illustrated in Fig. 1A. For any $|\lambda|<1$, the series converges to 0, and negative eigenvalues reflect a change of sign every beat. Thus, the most negative eigenvalue (λ_{alt}) is precisely the factor by which the most prominent alternating perturbation is multiplied after every beat. λ_{alt} represents an ideal marker of alternans, because it quantifies directly how an alternant perturbation decays over successive cycles. When the propensity to alternans increases, λ_{alt} decreases from 0 towards –1, which is the limit of dynamic stability. When $\lambda_{alt}=-1$, a perturbation no longer dissipates but keeps alternating.

We previously presented a theoretical framework forming the basis for an experimental estimation of λ_{alt} (Lemay *et al.* 2012). Central to this approach are pacing protocols comprising stochastic beat-to-beat variations of pacing cycle length. These stochastic perturbations continuously excite all the eigenmodes, but those with eigenvalues close to 0 dissipate rapidly while those with eigenvalues close to –1 tend to persist in an alternating manner, revealing the susceptibility to alternans.

Our aim in the present study was to demonstrate the practical usefulness of this approach in isolated cardiac myocytes. We show that the experimentally estimated value of λ_{alt} is an appropriate marker to quantify the propensity to alternans. In addition, we derived further markers to discriminate between voltage-driven and Ca^{2+}-driven alternans, and tested them in experiments and computer simulations using models of rabbit and human ventricular myocytes. Our results show that it is possible to discriminate between voltage-driven and Ca^{2+}-driven alternans with a sensitivity and specificity >80%, even when the propensity to alternans is moderate, thus permitting information to be gained regarding the ionic mechanism of alternans before alternans fully develops. This opens the perspective of implementing new strategies to evaluate the propensity to alternans, which, in a translational setting, would be of assistance for the prevention and the therapy of associated arrhythmias.

Methods

Ethical approval

All experiments (see protocols below) were conducted at the University of California, Los Angeles (UCLA). Animals were handled in accordance with the ethical principles and guidelines of UCLA Institutional Animal Care and Use Committee (ARC# 2003-063-33) and conformed to the Guide for the Care and Use of Laboratory Animals published by the US National Institutes of Health. The authors understand the ethical principles under which the journal operates. The present work complies with the animal ethics checklist of the journal.

Isolation of rabbit ventricular myocytes

Rabbit cardiac myocytes were isolated as previously (Madhvani *et al.* 2011). Briefly, hearts were rapidly excised from New Zealand White (NZW) male rabbits (age: 3-4

months, weight: 1.9-2.1 kg, n=21 rabbits) under deep anaesthesia induced by an intravenous injection of sodium pentobarbital (100 mg/kg) and heparin sulphate (1000 U). The adequacy of anaesthesia was confirmed by the lack of pedal withdrawal reflex, corneal reflex, and motor response to pain stimuli by scalpel tip. The hearts were placed in Ca^{2+}-free Tyrode's solution containing (in mmol/L) 140 NaCl, 5.4 KCl, 1 $MgCl_2$, 0.33 NaH_2PO_4, 10 glucose, and 10 HEPES adjusted to pH 7.4. The aorta was cannulated and the heart perfused retrogradely at 37°C on a Langendorff apparatus with Ca^{2+}-free Tyrode's buffer containing 1.65 mg/mL collagenase. All solutions were continuously bubbled with 95% O_2–5% CO_2. After enzymatic digestion, the hearts were swirled in a beaker to dissociate cells. The Ca^{2+} concentration was gradually increased to 1.8 mmol/L, and the cells were stored at room temperature. The animals were supplied by Charles River Laboratories (Wilmington, MA,USA) and maintained in cages with standard lab chow and water available *ad libitum*.

Patch clamp experiments

The myocytes were bathed in a solution containing (in mmol/L): 136 NaCl, 5.4 KCl, 1.8 $CaCl_2$, 1 $MgCl_2$, 0.33 NaH_2PO_4, 10 glucose, and 10 HEPES, adjusted to pH 7.4. Membrane potential was recorded (sampling rate: 10 kHz) at 34-36 °C using the whole-cell patch clamp technique in the current clamp mode using AxoPatch200B (Axon Instruments). The pipettes (resistance 1-2 MΩ) were filled with (in mmol/L): 110 K-aspartate, 30 KCl, 5 NaCl, 10 HEPES, 0.1 EGTA, 5 MgATP, 5 creatine phosphate, 0.05 cAMP adjusted to pH 7.2. In some experiments, ryanodine was added to the bath solution at a concentration of 100 µmol/L to completely suppress Ca^{2+} release from the sarcoplasmic reticulum. Additional experiments were performed using the perforated patch technique using amphotericin B (240 µg/mL) in the pipette solution.

Pacing protocols

Ramp protocol without stochastic variations: The cells were first paced with 2 ms current pulses at approximately twice the threshold of the resting cell for 3 min at a starting basic cycle length (CL) of 250-400 ms to allow for accommodation. Subsequently, CL was progressively decreased on a beat-to-beat basis over 10-25 min. To minimize transient alternans due to abrupt CL changes, the descending CL ramps were designed such that instantaneous pacing rate (1/CL) increases linearly with time.

Ramp protocol with stochastic variations: The series of pacing CLs were designed as described above and stochastic variations of CL (Gaussian distribution with zero mean and a standard deviation (SD) of 10 ms if not specified otherwise) were implemented to the entire CL series.

Computer simulations of action potentials

Computer simulations were conducted with the Mahajan *et al*. rabbit ventricular cell model (Mahajan *et al.* 2008), which corresponds directly to our experimental preparation, and the O'Hara-Virag-Varró-Rudy (ORd) human ventricular cell model (O'Hara *et al.* 2011). The models were subjected to similar pacing protocols.

The Mahajan *et al*. model was run using a constant time step of 0.005 ms. Gating variables were integrated using the method of Rush and Larsen, the state occupancies of the Markovian model of the L-type Ca^{2+} channel were computed as described by Milescu *et al*. (Milescu *et al.* 2005) and membrane potential and ion concentrations were integrated using the forward Euler algorithm. The ORd model (MATLAB source code downloaded from Dr. Rudy's website www.rudylab.edu) was run using the "ode15s" MATLAB ordinary differential equation solver.

Analysis of APD, DI and CL series and markers of alternans

In experiments and simulations, activation was defined for every action potential (AP) at –35 mV during depolarization and APD was determined at a potential 10 mV above the minimal diastolic potential preceding the AP. Series of consecutive APDs, DIs and CLs

(APD_n, DI_n, CL_n) were derived from these fiducial time points with the convention $CL_n=APD_n+DI_n$ (Lemay *et al.* 2012). In this convention, DI_{n-1} is the DI immediately before APD_n (which occurs during CL_n), and DI_n is the DI immediately after APD_n.

Markers to characterize alternans were derived starting from the notion that APD depends on several previous DIs and APDs ("memory" (Kalb *et al.* 2004; Kalb *et al.* 2005; Mironov *et al.* 2008)). This dependence can be formalized as a generalized restitution function *g* (Kalb *et al.* 2005):

$$APD_n = g(DI_{n-1}, APD_{n-1}, DI_{n-2}, APD_{n-2}, ...).$$

Because CL was explicitly controlled in our study, we expressed the generalized restitution function in terms of APD and CL as

$$APD_n = f(APD_{n-1}, CL_{n-1}, APD_{n-2}, CL_{n-2}, ...).$$

Assuming that beat-to-beat variations of APD and CL are small enough such that nonlinearities of *f* are not involved, one can linearize *f* around mean APD and CL values as (Kalb *et al.* 2005; Lemay *et al.* 2012):

$$\delta APD_n = \alpha_1 \delta APD_{n-1} + \alpha_2 \delta APD_{n-2} + ... + \beta_1 \delta CL_{n-1} + \beta_2 \delta CL_{n-2} + ... + \varepsilon_n,$$

where δAPD_n and δCL_n are the respective deviations of APD_n and CL_n from their local mean values and ε_n is an noise term representing intrinsic fluctuations of APD arising, e.g., from stochastic channel gating (Zaniboni *et al.* 2000; Lemay *et al.* 2011), stochastic Ca^{2+}-induced Ca^{2+} release (Cannell *et al.* 2013) or noise in the measuring apparatus. The coefficients α_i and β_i quantify the response of APD to a perturbation of the i^{th} previous APD or CL and correspond respectively to the partial derivatives $\partial f/\partial APD_{n-i}$ and $\partial f/\partial CL_{n-i}$, respectively.

The above equation represents a discrete-time autoregressive-moving-average (ARMA) model (Ljung 1999) taking the series of (controlled) CLs as input and producing the series of (measured) APDs as output. The coefficients α_i and β_i characterize this input-output behaviour of the investigated cardiac cell. If CL variations are absent or negligible (e.g., CL is kept constant), the system reduces to an autoregressive (AR) model, in which the contributions of the coefficients β_i are lost:

$$\delta APD_n = \alpha_1 \delta APD_{n-1} + \alpha_2 \delta APD_{n-2} + ... + \varepsilon_n .$$

To illustrate this with a few examples, we first consider the immediate response of APD to an isolated perturbation of CL applied during steady state pacing (e.g., S1S2 protocol). In this situation, for the APD immediately following the perturbation and neglecting the noise term, the equation becomes $\delta APD_n = \beta_1 \delta CL_{n-1}$. Therefore, the first moving average coefficient β_1 directly reflects the conventional instantaneous S1S2 restitution slope. Second, we consider a setting in which alternans is principally determined by the kinetics of membrane currents during the previous DI (voltage-driven alternans). In such a situation, APD variations are strongly influenced by β_1, in agreement with classical restitution theory. In contrast, if alternans is caused predominantly by fluctuations of the Ca^{2+} transient (due, e.g., to variations of sarcoplasmic Ca^{2+} loading and release) which are indirectly transmitted to APD, the latter will be predominantly governed by the autoregressive coefficients α_i while the β_i's will remain relatively small and exert only a weak effect. However, the α_i's and β_i's cannot be ascribed directly to either the voltage or the Ca^{2+} driving mechanism (a detailed analysis is presented below in the section "Insights from an iterated map model").

Given a series of CLs and APDs, the coefficients α_i and β_i can be estimated using dedicated algorithms (Ljung 1999). However, further analysis is required to extract information about alternans and stability. As we showed previously (Lemay *et al.* 2012), by applying a *Z*-transform to the equation of the ARMA model, so-called transfer functions can be derived to characterize the response of the cell in the frequency domain as well the stability of this response:

$$H_{CL\to APD}(z)=\frac{\beta_1 z^{-1}+\beta_2 z^{-2}+\ldots}{1-\alpha_1 z^{-1}-\alpha_2 z^{-2}-\ldots}$$

$$H_{CL\to DI}(z)=1-H_{CL\to APD}(z)=\frac{1-(\alpha_1+\beta_1)z^{-1}-(\alpha_2+\beta_2)z^{-2}-\ldots}{1-\alpha_1 z^{-1}-\alpha_2 z^{-2}-\ldots}.$$

The roots of the denominator, called "poles" or "eigenvalues" (λ), determine the stability of the system. The system is stable only if $|\lambda|<1$ for all λ's (Ljung 1999). For a cell prone to alternans, one of the eigenvalues will dominate and approach –1 when alternans is imminent. This eigenvalue (λ_{alt}) thus characterizes the propensity to alternans. It can be understood as the number by which a perturbation of APD is scaled before being transmitted to the next beat (Fig. 1A).

The roots of the numerators, called "zeros" (ζ), determine the phase relationships between CL and APD variations. While the zeros do not provide information on stability, they nevertheless allow untangling the relative contributions of the coefficients α_i and β_i to the alternating behaviour of APD. Therefore, the major advantage of introducing controlled stochastic variations of pacing CL is to permit the estimation of the coefficients β_i, which are necessary to provide a full picture of the dynamic response of APD, not only in terms of the susceptibility to alternans but also in terms of the underlying dynamics.

We analysed the series of APDs, DIs and CLs using a sliding window (unless specified otherwise: 100 beats slid in steps of 25 beats). For each window, the series were first detrended using a 2nd degree polynomial. Then, a 2nd order AR model (protocols without stochastic CL variations) or ARMA model (protocols with stochastic CL variations) was used to fit the data (Ljung 1999). λ_{alt} was defined as the eigenvalue closest to –1. While λ_{alt}=–1 represents full persistent alternans, values close to but still >–1 already indicate the susceptibility to alternate (see Fig. 1A). We therefore defined thresholds of –0.5 and –0.8 for a moderate and a high susceptibility to alternans, respectively. We showed in previous computational work (Lemay *et al.* 2012) that the dominant zero of $H_{\mathrm{CL}\to\mathrm{DI}}$ (ζ_{alt}) is near 0 if alternans is voltage-driven, whereas it is close to λ_{alt} if alternans is Ca^{2+}-driven. The zero ζ_{alt}

and the difference ζ_{alt}–λ_{alt} thus represent markers of the primary mechanism of alternans. Our analysis thus reports λ_{alt} (susceptibility to alternans), and, for protocols with stochastic CL variations, ζ_{alt}, ζ_{alt}–λ_{alt} and β_1 (further markers characterizing the dynamics of alternans). In addition, mean APD was plotted vs. mean DI in each window to generate a dynamic restitution curve. The slope of the plot provides an estimate of the dynamic restitution slope (Kalb *et al.* 2004; Tolkacheva *et al.* 2006).

The ARMA model is a good approximation of the generic APD restitution function under the assumption that APD and CL variations around their mean values remain small enough such that nonlinearities remain weak. Hence, for the linear analysis using the ARMA model to remain applicable, the stochastic variations of pacing CL must be kept small enough such that nonlinearities remain weak. If nonlinearities need to be accounted for, the analysis can be extended with nonlinear terms (Armoundas *et al.* 2002; Dai & Keener 2012). However, this approach would have the disadvantage that more data (longer series of APDs/CLs) would be required to obtain reliable nonlinear model identification.

All analyses and simulations were conducted using MATLAB (The MathWorks, Natick, MA, USA). AR and ARMA models were identified using a least squares algorithm (function “armax” from the MATLAB System Identification Toolbox).

Statistics

The ability of ζ_{alt}, and β_1 to discriminate between control experiments and experiments with ryanodine was evaluated in terms of specificity and sensitivity by computing receiver operating characteristic curves.

Insights from an iterated map model

It must be noted that the coefficients α_i and β_i and the markers λ_{alt} and ζ_{alt} are interrelated and cannot be ascribed either to voltage-driven or to Ca^{2+}-driven alternans. Furthermore, in a physiological setting, alternans is never either fully voltage-driven or fully Ca^{2+}-driven. While one mechanism typically predominates, both mechanisms contribute jointly to the

genesis of alternans (Edwards & Blatter 2014; Groenendaal *et al.* 2014). To gain deeper insights into the relationships between λ_{alt}, ζ_{alt}, and β_1 during Ca^{2+}-driven vs. voltage-driven alternans, we investigated the following iterated map model (Fig. 1B) implementing the interactions between the AP and the Ca^{2+} transient (δ denotes a small deviation from the mean):

$$\delta APD_n = \mu \cdot \delta APD_{n-1} + \rho \cdot \delta CT_n + \nu \cdot \delta CL_{n-1} + \varepsilon_{APD,n}$$
$$\delta CT_n = \gamma \cdot \delta CT_{n-1} + \varphi \cdot \delta APD_{n-1} + \kappa \cdot \delta CL_{n-1} + \varepsilon_{CT,n}$$

where CT_n is the peak of the Ca^{2+} transient during the n^{th} action potential. In the first equation and as illustrated in Fig. 1B, μ and ν describe the dependence of APD on the previous APD and CL independently of the Ca^{2+} transient and ρ describes the specific contribution of the Ca^{2+} transient in determining APD, which reflects Ca^{2+} to APD coupling. For $\rho>0$ (positive Ca^{2+} to APD coupling), a larger Ca^{2+} transient leads to a longer APD, whereas for $\rho<0$ (negative Ca^{2+} to APD coupling), a larger Ca^{2+} transient leads to a shorter APD. In the second equation, γ represents the feedback of CT on itself, φ represents the influence of APD on the next Ca^{2+} transient (APD to Ca^{2+} coupling), and κ is a parameter describing the direct effect of a change of CL on the next Ca^{2+} transient (CT restitution). This latter parameter is expected to be positive, because shortening CL results in a smaller Ca^{2+} transient during the next AP since the sarcoplasmic reticulum has less time to refill and since the recovery of the L-type Ca^{2+} current from inactivation may still be incomplete. Most cardiac cell models reproduce this behavior. $\varepsilon_{APD,n}$ and $\varepsilon_{CT,n}$ are corresponding error terms.

Although this map model is a simplification of the detailed ionic mechanisms shaping APD and the Ca^{2+} transient, it offers the advantage to be tractable analytically.

Case of principally Ca^{2+}-driven alternans

If alternans is essentially driven by unstable Ca^{2+} cycling rather than by the voltage-dependent kinetics of membrane currents, μ and ν are small and APD variations reflect the

variations of the Ca^{2+} transient via the parameter ρ. If the contributions from μ and v are neglected, the system reduces to

$$\begin{aligned}\delta APD_n &= \rho \cdot \delta CT_n + \varepsilon_{APD,n} \\ \delta CT_n &= \gamma \cdot \delta CT_{n-1} + \varphi \cdot \delta APD_{n-1} + \kappa \cdot \delta CL_{n-1} + \varepsilon_{CT,n}\end{aligned}.$$

Combining both equations (neglecting the error terms) and solving for δAPD_n, we obtain:

$$\delta APD_n = (\gamma + \varphi \cdot \rho) \cdot \delta APD_{n-1} + \rho \cdot \kappa \cdot \delta CL_{n-1},$$

which corresponds to an ARMA model with $\alpha_1 = \gamma+\varphi\rho$ and $\beta_1 = \rho\kappa$.
Using Z-transformation, the transfer functions $H_{CL\rightarrow APD}(z)$ and $H_{CL\rightarrow DI}(z)$ are obtained as

$$H_{CL\rightarrow APD}(z) = \frac{\rho\kappa z^{-1}}{1-(\gamma+\rho\varphi)z^{-1}} \text{ and } H_{CL\rightarrow DI}(z) = 1 - H_{CL\rightarrow APD}(z) = \frac{1-(\gamma+\rho\varphi+\rho\kappa)z^{-1}}{1-(\gamma+\rho\varphi)z^{-1}}.$$

The pole λ_{alt} and the zero ζ_{alt} of $H_{CL\rightarrow DI}(z)$ are

$$\begin{aligned}\lambda_{alt} &= \gamma + \rho\varphi \\ \zeta_{alt} &= \gamma + \rho\varphi + \rho\kappa,\end{aligned}$$

and the difference $\zeta_{alt}-\lambda_{alt}$ is

$$\zeta_{alt} - \lambda_{alt} = \rho\kappa.$$

This result indicates that Ca^{2+}-driven alternans is caused by $\lambda_{alt} = \gamma+\rho\varphi$ approaching –1, and because $\kappa>0$, the sign of $\zeta_{alt}-\lambda_{alt}$ permits to infer the sign of ρ, i.e., the sign of Ca^{2+} to APD coupling.

Case of principally voltage-driven alternans

Conversely, if alternans is essentially voltage-driven, the parameter ρ becomes negligible and the iterative map model for alternans reduces to

$$\delta APD_n = \mu \cdot \delta APD_{n-1} + \nu \cdot \delta CL_{n-1} + \varepsilon_{APD,n},$$

i.e., to an ARMA model with $\alpha_1 = \mu$ and $\beta_1 = \nu$, with corresponding transfer functions

$$H_{CL\to APD}(z) = \frac{\nu z^{-1}}{1-\mu z^{-1}} \qquad \text{and} \qquad H_{CL\to DI}(z) = 1 - H_{CL\to APD}(z) = \frac{1-(\mu+\nu)z^{-1}}{1-\mu z^{-1}}.$$

The pole λ_{alt} and the zero ζ_{alt} of $H_{CL\to DI}(z)$ are

$$\lambda_{alt} = \mu \qquad \text{and} \qquad \zeta_{alt} = \mu + \nu.$$

Thus, the difference ζ_{alt}–λ_{alt} is ν, which corresponds to β_1. Thus, in the classical alternans model (Nolasco & Dahlen 1968), ν corresponds to the S1S2 restitution slope and is expected to be close to 1 at the onset of alternans. Since λ_{alt} is then expected to be –1, we expect that ζ_{alt} will be around 0 in the case of essentially voltage-driven alternans.

Mixed case

If both voltage and Ca^{2+} dynamics contribute to alternans to a similar extent, ζ_{alt}, λ_{alt} and β_1 become more complicated functions which are less straightforward to link to the parameters of the iterated map model. However, we expect a continuum of possible values for ζ_{alt}, λ_{alt} and β_1.

Results

λ_{alt} quantifies the susceptibility to alternans even without stochastic cycle length variations

The APD series of a ventricular myocyte subject to a ramp pacing protocol without stochastic variations is shown in Fig. 2*A*. The progressive decrease of CL led to an overall APD decrease and eventually resulted in manifest alternans. The insets in Fig. 2*A* and the corresponding APs shown in Fig. 2*B* illustrate that alternans is difficult to identify by visual inspection before its full development. These insets also depict the intrinsic beat-to-beat variability of APD. In Fig. 2*A*, λ_{alt} is shown with different background colours based on the thresholds defined in the Methods section (green: $\lambda_{alt}>-0.5$, low susceptibility; orange: $-0.5>\lambda_{alt}>-0.8$, moderate susceptibility; red: $\lambda_{alt}<-0.8$, high susceptibility). λ_{alt} decreased from around –0.2 to –1. Intermittent alternans appeared in the form of bursts of alternation when λ_{alt} reached –0.8 (inset), followed by full sustained alternans, hence motivating the selection of a threshold of –0.8 as a marker of the imminence of alternans. Fig. 2*C* shows the dynamic restitution curve for this experiment. Globally, the dynamic restitution slope remained <1.

The ramp protocol was conducted with 7 cells (from 3 animals). In 6 out of these 7 cells, λ_{alt} decreased progressively during the ramp protocol and alternans appeared when λ_{alt} reached –0.8, although the APD and CL at which alternans appeared was different between the individual cells. This indicates that λ_{alt} reflects the propensity to alternans, and is not linked to a given APD or CL. In one cell, alternans did not develop although CL was decreased to 150 ms at the end of the protocol, and λ_{alt} did not decrease below –0.5.

Stochastic cycle length variations provide insight into the mechanisms governing alternans

Fig. 3 illustrates an experiment in which a myocyte was subjected to a ramp protocol with stochastic variations. With this protocol, λ_{alt} progressively decreased as well. Sustained alternans developed around beat number 2600 when λ_{alt} reached –0.8. In contrast to cells paced without stochastic variations (e.g., Fig. 2), sustained alternans was then

characterized by occasional phase reversals, visible as transitions between periods in which even APDs were longer than odd APDs (marked in different colours) and periods in which odd APDs were longer than even APDs. These phase reversals occurred irregularly. During the descending CL ramp, APD exhibited a progressive trend to alternate (Fig 3*A*, insets), with bursts of alternans that lasted progressively longer in response to the continuous perturbations caused by stochastic pacing.

Importantly, incorporating stochastic CL variations permitted the estimation of two additional markers, β_1 and ζ_{alt}. β_1 (corresponding to the conventional S1S2 restitution slope), slightly increased during the experiment and reached 0.2 at the onset of alternans, i.e., <<1. Interestingly, ζ_{alt} decreased gradually in parallel with λ_{alt}, but it always remained slightly more positive. Consequently, the difference ζ_{alt}–λ_{alt} was positive but remained close to 0. These relations between β_1, ζ_{alt} and λ_{alt} are further illustrated in Fig. 3*B* (ζ_{alt} vs. λ_{alt}) and Fig. 3*C* (β_1 vs. λ_{alt}). Fig. 3*B* shows that ζ_{alt} evolved along the diagonal defined by ζ_{alt}=λ_{alt} but remained above it, and Fig. 3*C* shows that β_1 remained near 0. The dynamic restitution slope (Fig. 3*D*) was approx. 0.5 at the onset of alternans, i.e., <<1.

Similar results were observed in 8 out of 10 cells (from 6 animals), in which λ_{alt} reached –0.8 when alternans developed. In these experiments, ζ_{alt} followed a course similar to λ_{alt} but always remained >λ_{alt} (ζ_{alt}–λ_{alt} always positive), and β_1 followed a course near 0 (β_1<0.5). The observation that ζ_{alt} remained close to λ_{alt} suggests that alternans was Ca^{2+}-driven in these experiments (Lemay *et al.* 2012), and the positive sign of ζ_{alt}–λ_{alt} indicates that Ca^{2+} to APD coupling was positive. In one of the 10 cells, the seal was lost before the end of the pacing protocol; alternans had not developed and λ_{alt} remained >–0.8. Interestingly, in one other cell that exhibited alternans, ζ_{alt} also followed a course similar to λ_{alt} but ζ_{alt}–λ_{alt} was negative, suggesting according to theory (Lemay *et al.* 2012) that Ca^{2+} to APD coupling was negative in this particular cell.

Ryanodine changes the dynamics governing alternans

It is established that Ca^{2+}-driven alternans results from unstable cycling of intracellular Ca^{2+}, especially due to a steep relation linking Ca^{2+} influx and sarcoplasmic Ca^{2+} load to

Ca^{2+} release (Qu *et al.* 2010). Because the ryanodine receptor is a central element in Ca^{2+}-induced Ca^{2+} release, we evaluated the behaviour of APD and the different markers during similar stochastic ramp experiments in the presence of ryanodine (100 µmol/L).

Ryanodine caused APD shortening and alternans occurred at shorter cycle lengths. Therefore, the standard deviation of the stochastic pacing interval variations was reduced to 3-5 ms. Fig. 4 illustrates a representative experiment with ryanodine. In this example, λ_{alt} progressively decreased until sustained alternans developed (around beat 2350) when λ_{alt} reached –0.8. However, ζ_{alt} did not decrease conjointly with λ_{alt} but fluctuated around 0 during the entire experiment, whereas β_1 and λ_{alt}–ζ_{alt} increased towards +1. Fig. 4*B* shows that ζ_{alt} remained around 0 independently of λ_{alt}, and Fig. 4*C* shows that β_1 evolved along the diagonal defined by β_1=–λ_{alt}. As in experiments without ryanodine, alternans exhibited irregularly occurring phase reversals once it had fully developed. These phase reversals thus appeared as a consequence of the stochastic CL variations. The dynamic restitution slope at the onset of alternans (Fig. 4*D*) was approx. 0.8, i.e., close to 1.

Out of 15 cells (from 9 animals) exposed to ryanodine, manifest alternans with λ_{alt}<–0.8 was observed in 4 cells. In these experiments, ζ_{alt} always remained close to 0 and ζ_{alt}–λ_{alt} increased above 0.5. In 10 of the remaining 11 cells, λ_{alt} nevertheless decreased to values <–0.5, APD exhibited intermittent bursts of alternans, and the tendency of ζ_{alt} to remain near 0 and of β_1 to increase was also observed. Thus, ryanodine changed the dynamics governing alternans and the relationship between the stochastic CL series and the resulting APD series in a manner compatible with a switch from essentially Ca^{2+}-driven to essentially voltage-driven alternans.

In a next step, we examined the capability of the markers ζ_{alt} and β_1 to discriminate between experiments with and without ryanodine. Because APD at the onset of alternans was different for every cell, we conducted this analysis independently of APD and CL by considering only the relationships between ζ_{alt}, β_1 and λ_{alt}. For this purpose, we pooled the results of all the estimations of these three markers in all experiments (including experiments in which sustained alternans was not observed), as shown in Fig. 5*A*. In the plot of ζ_{alt} vs. λ_{alt}, the distribution of the points and the regression lines for ryanodine vs. control experiments confirm that ζ_{alt} followed λ_{alt} in control experiments whereas it

remained near 0 in the presence of ryanodine. The plot of β_1 vs. λ_{alt} confirms that β_1 changed only moderately in control experiments whereas it followed the diagonal $\beta_1=-\lambda_{alt}$ in the presence of ryanodine. To analyse the discriminating capability of ζ_{alt} and β_1 in terms of specificity and sensitivity, the data were collected in bins of λ_{alt} with a width of 0.1, and a receiver operating characteristic curve was constructed for each bin, as illustrated in Fig. 5*B*. This analysis shows that the specificity and sensitivity of ζ_{alt} and β_1 (calculated from a single series of 100 consecutive CLs and APDs) to discriminate between the presence and the absence of ryanodine reaches >80% when $\lambda_{alt}<-0.4$ and increases with λ_{alt} approaching –1. Since the discrimination threshold cannot be determined a priori, we also determined in Fig. 5*C* the specificity and sensitivity of the criteria $\zeta_{alt}>0.5\cdot\lambda_{alt}$ and $\beta_1>-0.6\cdot\lambda_{alt}$ (illustrated by the green dotted lines in Fig. 5*A*). Overall, ζ_{alt} was more specific and β_1 more sensitive, and the sensitivity/specificity was >80% even for $\lambda_{alt}>-0.5$, i.e. for a low susceptibility to alternans without any manifest alternation in APD time series.

To ascertain whether excessive cell dialysis could affect the results, additional experiments (2 under control conditions, 2 with 100 µmol/L ryanodine) were conducted using the perforated patch technique. Similar behaviours of the different markers were observed, suggesting that using the ruptured patch technique did not alter the main outcomes of the analyses.

Computer simulations confirm experimental observations

To gain deeper insights into the progression to alternans during the ramp protocols and to support the notion of a switch from principally Ca^{2+}-driven to principally voltage-driven alternans when the ryanodine receptor is blocked, we ran computer simulations using the Mahajan *et al*. rabbit ventricular myocyte model (Mahajan *et al.* 2008), which corresponds to our experimental preparation and which was especially developed to replicate the APD restitution curves observed experimentally as well as the alternans of APD and the Ca^{2+} transient at rapid pacing rates.

Fig. 6 illustrates a simulation of a ramp protocol with stochastic variations. Alternans of APD appeared in bursts before becoming persistent at the end of the simulation. However,

the peak of the Ca^{2+} transient exhibited bursts of alternans already early in the simulation, before APD alternans became manifest (insets in Fig. 6*A*), indicating that alternans originated initially from unstable Ca^{2+} cycling and resulted later in visible APD alternans. The progression of λ_{alt} and ζ_{alt} during acceleration of pacing was similar to that in the experiments without ryanodine, with ζ_{alt} following λ_{alt} but being always less negative. The difference ζ_{alt}–λ_{alt} always remained in the interval between 0 and 0.2. The marker β_1 remained low as well. At the onset of APD alternans, when λ_{alt} reached –0.8, ζ_{alt}–λ_{alt} was 0.06 and β_1 amounted to 0.07. The slope of the dynamic restitution curve (Fig. 6*D*) remained in the range 0.4-0.6 during the entire protocol.

To test whether Ca^{2+} cycling could be stabilized and the regime of alternans switched from essentially Ca^{2+}-driven to essentially voltage-driven, we simulated the application of ryanodine by decreasing the strength of the Ca^{2+} release current through ryanodine receptors (g_{RyR}) by 90%, as illustrated in Fig. 7. As in the experiments, APD was decreased by this intervention and a ramp protocol descending to CLs < 100 ms was used, with stochastic variations having a SD of 2 ms. Similar to the control model, λ_{alt} gradually decreased towards –1 until full alternans developed. However, the peaks of the Ca^{2+} transients exhibited manifest alternans only in conjunction with APD alternans (insets). Furthermore, as in the experiments with ryanodine, ζ_{alt} clearly remained close to 0 and, consequently, ζ_{alt}–λ_{alt} increased to 1. β_1 increased to 1 as well. The dynamic restitution slope was steeper than in the control model (maximal slope: 1.1; slope at the onset of alternans: 0.7; Fig. 7*D*). This behaviour of β_1, ζ_{alt} and the dynamic restitution slope (close to 1, 0 and 1, respectively) is in agreement with voltage-driven alternans, i.e., with a steep dependence of APD on the previous DI as proposed in classical restitution theories.

Thus, in terms of λ_{alt}, ζ_{alt}, β_1 and dynamic restitution slope, the behaviour of the Mahajan *et al*. model was very consistent with that observed in the experiments, and decreasing g_{RyR} by 90% clearly changed the dynamics of alternans and switched its mechanism from principally Ca^{2+}-driven to principally voltage-driven. In the experiments, we used a high ryanodine concentration that blocks Ca^{2+} release and leads to Ca^{2+} accumulation in the sarcoplasmic reticulum (SR). This accumulation was confirmed in the Mahajan *et al*. model. This resulted in relatively smaller variations of [Ca^{2+}] in the SR during the AP

cycle, which, in turn, decreased Ca^{2+} release fluctuations. The feedback mechanism that causes Ca^{2+}-driven alternans was therefore depressed.

To evaluate the robustness of our approach, we ran the simulations shown in Figs. 6 and 7 ten times with the same descending ramps but with different realizations of the stochastic variations of CL and analysed λ_{alt}, ζ_{alt}, β_1 and ζ_{alt}–λ_{alt} in terms of mean and SD over the 10 different runs. There were subtle differences from run to run, but the mean behaviour of the alternans markers was similar and consistent with the individual simulations shown in Figs. 6 and 7. The SD of the markers was typically in the range of 0.1 far from the alternans regime and the SD of λ_{alt} strongly decreased when λ_{alt} approached –1. We also examined the effect of changing the SD of the stochastic CL variations. When these variations were decreased by half, the average behaviour of the markers was similar, and their SD was lower. However, when the SD of CL variations was doubled, some stimuli applied after particularly short stochastic CLs failed to be captured because they fell within the refractory period. These observations suggest that in an experimental setting, the SD of CL variations should be optimized to provide a sufficient signal-to-noise ratio in the measured APD series without causing stimulation failure.

Ca^{2+}-driven alternans is also identified in a human ventricular cell model

To examine whether the stochastic pacing approach could also be applicable in the context of the human heart, we conducted simulations using the O'Hara *et al*. (ORd) human ventricular model (O'Hara *et al.* 2011). Fig. 8*A* illustrates the behaviour of APD, Ca^{2+} transient amplitude and alternans markers in the original control model (ramp descending from 1000 ms; SD of stochastic variations: 3 ms). To demonstrate the influence of Ca^{2+} dynamics on alternans generation, Fig. 8*B* shows the behaviour of the ORd model when the Ca^{2+} concentrations in all subcellular compartments were clamped to their initial values.

In the control model, alternant fluctuations of Ca^{2+} transient amplitude appeared before those of APD, and they were also more prominent. The decrease of λ_{alt}, towards –1 was accompanied by a parallel decrease of ζ_{alt} whereas β_1 and λ_{alt}–ζ_{alt}, remained <0.3, similar to the behaviour of the rabbit myocytes. This is in line with the notion that alternans is Ca^{2+}-

driven in the control model, as reported (O'Hara *et al.* 2011). Under conditions of Ca^{2+} clamp, APD was prolonged due to the missing Ca^{2+}-based inactivation of the L-type Ca^{2+} current. But importantly, the behaviour of ζ_{alt} (close to 0), of β_1 (close to 1) and λ_{alt}–ζ_{alt} (close to 1) during the decrease of λ_{alt} reflected the disappearance of Ca^{2+}-driven alternans and the appearance of voltage-driven alternans. The dynamic restitution slope (Fig. 8*C*) was larger in the Ca^{2+} clamped model than in the control model. The trajectories in the plots of ζ_{alt} vs. λ_{alt} and β_1 vs. λ_{alt} (Fig. 8*C*) were characteristic of Ca^{2+}-driven alternans in the control model and of voltage-driven alternans in the Ca^{2+}-clamped model. These results therefore suggest that Ca^{2+}-driven alternans can also be correctly identified in human ventricular myocytes using stochastic pacing protocols.

Discussion

We investigated the susceptibility to alternans of isolated rabbit ventricular myocytes by using a pacing protocol combining a progressive decrease of CL with stochastic CL variations. The analysis of the resulting sequences of APDs using an autoregressive-moving-average model permitted the experimental estimation of the eigenvalue λ_{alt}, which was shown in theoretical studies to be the ultimate marker of alternans (Li & Otani 2003; Groenendaal *et al.* 2014). Another innovative aspect of our analysis and the principal advantage of stochastic pacing is that it allows the extraction of further markers to characterize alternans (ζ_{alt}, ζ_{alt}–λ_{alt}, β_1).

In a previous computational study (Lemay *et al.* 2012), we showed that these markers exhibit distinctive signatures in a mathematical model which can be parameterized to exhibit voltage-driven or Ca^{2+}-driven alternans (Sato *et al.* 2006). To ascertain these distinct signatures experimentally, we used ryanodine to depress Ca^{2+}-induced Ca^{2+} release, a key player in Ca^{2+}-driven alternans (Qu *et al.* 2010; Edwards & Blatter 2014; Wagner *et al.* 2015). Our experiments demonstrated the theoretically anticipated change of ζ_{alt} and β_1 suggestive of a shift from Ca^{2+}-driven to voltage-driven alternans. Our findings are consistent with the notion that rabbit ventricular myocytes are prone to Ca^{2+}-driven

alternans, as shown recently using dual voltage and Ca^{2+} recordings (Kanaporis & Blatter 2015).

We also found that ζ_{alt} and β_1 discriminated between the presence and absence of ryanodine with a specificity and sensibility reaching already ~80% when the propensity to alternans was low (λ_{alt}>–0.5). Therefore, our approach can not only serve to detect the imminence of alternans by using λ_{alt}, but also to identify whether it is prone to occur via a Ca^{2+}-driven or voltage-driven mechanism.

Further support to our approach was provided by simulations with the Mahajan *et al*. model of the rabbit ventricular myocyte (Mahajan *et al.* 2008), which was specifically developed to replicate APD dynamics and the Ca^{2+} cycling behaviour during rapid pacing. The behaviour of λ_{alt}, ζ_{alt} and β_1 in the model was consistent with our experimental observations. We then conducted simulations using a recent model of the human ventricular myocyte. The simulations suggest that it should also be possible to identify Ca^{2+}-driven alternans in human ventricular myocytes using stochastic pacing protocols.

Our work finally shows that conventional restitution slopes are poor markers to identify the occurrence of alternans (except in the case of a purely voltage-driven mechanism without memory of previous pacing cycles as in classical restitution theory (Nolasco & Dahlen 1968; Guevara *et al.* 1981; Chialvo *et al.* 1990)). This further stresses the importance of revisiting the classical restitution concept in the genesis of alternans.

It must be underlined that both voltage and Ca^{2+} driving mechanisms contribute jointly to varying degrees to the generation of alternans rather than only one or the other (Edwards & Blatter 2014; Groenendaal *et al.* 2014). In the experiments, the mechanisms of unstable voltage dynamics that were revealed by the application of ryanodine were presumably present before, and they were certainly present in the simulations since the formulation of membrane currents was not changed. It is possible that both our experiments and simulations represented situations in which one mechanism clearly outweighed the other, and, in future studies, it would therefore be adequate to also investigate situations in which both mechanisms contribute to alternans to a similar extent and how our alternans markers evolve during a gradual transition from one to the other mechanism.

Extension of the analytical framework from cell to organ

In this study, we conducted experiments with single cells. In intact tissue, electrotonic interactions and conduction velocity restitution may further influence the mechanisms of alternans and give rise, e.g., to spatially discordant patterns (Qu *et al.* 2010). While this adds a level of complexity to the mechanisms underlying alternans, it does not preclude the validity of our analytical method. Indeed, dominant eigenvalue analysis based on principal components analysis or maximum likelihood estimation has recently been proposed (Petrie & Zhao 2012) and successfully applied (Kakade *et al.* 2013) on optical recordings of membrane potential in whole hearts during a perturbed downsweep protocol. Moreover, in clinical studies, QT interval stability analysis based on the magnitude of eigenvalues obtained via autoregressive modelling of the QT interval was shown to correlate with the propensity to ventricular tachyarrhythmias (Chen *et al.* 2011). These studies therefore suggest that our method is also applicable at the multicellular tissue and organ levels. We postulate that stochastic pacing may actually render it more reliable by continuously exciting the dominant eigenmodes that need to be identified. A recent study (Dvir & Zlochiver 2013) suggests that stochastic pacing in itself reduces the propensity to alternans and even prevents the transition to spatially discordant alternans by shifting the APD restitution slope, an effect explained on the basis of nonlinear switched system theory. In a translational context, stochastic pacing could therefore be used both as a diagnostic and preventive measure.

Nevertheless, these different aspects will require to be carefully evaluated in further studies. Such investigations are needed to clarify whether our approach can be used gainfully in the setting of the human heart. In this situation, it should be underlined that the recorded signal (electrogram or ECG) should be of sufficient duration and sampled at a sufficiently high rate to capture small APD or QT interval variations in the millisecond range. To deploy the maximal efficiency of ARMA model identification, cardiac CL series should also be fully uncorrelated (which is not the case during sinus rhythm or conventional pacing protocols). When full alternans appears during stochastic pacing, nonlinear model identification can then be applied to provide further insights into the

characteristics of the period-doubling bifurcation (Armoundas *et al.* 2002; Dai & Keener 2012).

Limitations

It was recently suggested that at the subcellular level, Ca^{2+}-driven alternans results from the interplay of the randomness of Ca^{2+} spark activation, the refractoriness of Ca^{2+} release units and spark recruitment (Qu *et al.* 2010). Mechanistically, Ca^{2+}-driven alternans can also involve early afterdepolarizations (Qu *et al.* 2010). We have not tested whether our approach can discriminate between these different factors.

Our study also has the limitation that we recorded APs but not Ca^{2+} transients. For this reason, we could not quantify the exact relative contribution of Ca^{2+}-driven and voltage-driven alternans. A recent study (Groenendaal *et al.* 2014) conducted using simultaneous voltage and Ca^{2+} recordings showed that both unstable Ca^{2+} cycling and unstable ion channel dynamics contribute together to alternans; however, at the limit determined by λ_{alt}=–1, one mechanism typically predominates. Simultaneous recording of voltage and Ca^{2+} thus offers an important tool for future studies. Nevertheless, our approach has the advantage that it can discriminate between Ca^{2+} and voltage-driven alternans without the need to measure Ca^{2+} transients, which would hardly be feasible in a clinical setting.

Conclusion

Eigenmode analysis is emerging as a highly valuable tool to probe the dynamics of cardiac electrophysiological systems. The potential of this approach deserves to be explored further and opens prospects for future basic and translational research.

References

Armoundas AA, Ju K, Iyengar N, Kanters JK, Saul PJ, Cohen RJ & Chon KH (2002). A stochastic nonlinear autoregressive algorithm reflects nonlinear dynamics of heart-rate fluctuations. *Ann Biomed Eng* **30,** 192-201.

Cannell MB, Kong CH, Imtiaz MS & Laver DR (2013). Control of Sarcoplasmic Reticulum Ca^{2+} Release by Stochastic RyR Gating within a 3D Model of the Cardiac Dyad and Importance of Induction Decay for CICR Termination. *Biophys J* **104,** 2149-2159.

Chen X, Hu Y, Fetics BJ, Berger RD & Trayanova NA (2011). Unstable QT interval dynamics precedes ventricular tachycardia onset in patients with acute myocardial infarction: a novel approach to detect instability in QT interval dynamics from clinical ECG. *Circ Arrhythm Electrophysiol* **4,** 858-866.

Chialvo DR, Gilmour RF, Jr. & Jalife J (1990). Low dimensional chaos in cardiac tissue. *Nature* **343,** 653-657.

Cram AR, Rao HM & Tolkacheva EG (2011). Toward prediction of the local onset of alternans in the heart. *Biophys J* **100,** 868-874.

Dai S & Keener JP (2012). Using noise to determine cardiac restitution with memory. *Phys Rev E Stat Nonlin Soft Matter Phys* **85,** 061902.

Dvir H & Zlochiver S (2013). Stochastic cardiac pacing increases ventricular electrical stability - a computational study. *Biophys J* **105,** 533-542.

Echebarria B & Karma A (2002). Instability and spatiotemporal dynamics of alternans in paced cardiac tissue. *Phys Rev Lett* **88,** 208101.

Edwards JN & Blatter LA (2014). Cardiac alternans and intracellular calcium cycling. *Clin Exp Pharmacol Physiol* **41,** 524-532.

Franz MR, Jamal SM & Narayan SM (2012). The role of action potential alternans in the initiation of atrial fibrillation in humans: a review and future directions. *Europace* **14 Suppl 5,** v58-v64.

Gizzi A, Cherry EM, Gilmour RF, Jr., Luther S, Filippi S & Fenton FH (2013). Effects of pacing site and stimulation history on alternans dynamics and the development of complex spatiotemporal patterns in cardiac tissue. *Front Physiol* **4,** 71.

Groenendaal W, Ortega FA, Krogh-Madsen T & Christini DJ (2014). Voltage and calcium dynamics both underlie cellular alternans in cardiac myocytes. *Biophys J* **106,** 2222-2232.

Guevara MR, Glass L & Shrier A (1981). Phase locking, period-doubling bifurcations, and irregular dynamics in periodically stimulated cardiac cells. *Science* **214,** 1350-1353.

Kakade V, Zhao X & Tolkacheva EG (2013). Using dominant eigenvalue analysis to predict formation of alternans in the heart. *Phys Rev E Stat Nonlin Soft Matter Phys* **88,** 052716.

Kalb SS, Dobrovolny HM, Tolkacheva EG, Idriss SF, Krassowska W & Gauthier DJ (2004). The restitution portrait: a new method for investigating rate-dependent restitution. *J Cardiovasc Electrophysiol* **15,** 698-709.

Kalb SS, Tolkacheva EG, Schaeffer DG, Gauthier DJ & Krassowska W (2005). Restitution in mapping models with an arbitrary amount of memory. *Chaos* **15,** 23701.

Kanaporis G & Blatter LA (2015). The mechanisms of calcium cycling and action potential dynamics in cardiac alternans. *Circ Res* **116,** 846-856.

Karagueuzian HS, Stepanyan H & Mandel WJ (2013). Bifurcation theory and cardiac arrhythmias. *Am J Cardiovasc Dis* **3,** 1-16.

Koller ML, Riccio ML & Gilmour RF, Jr. (1998). Dynamic restitution of action potential duration during electrical alternans and ventricular fibrillation. *Am J Physiol* **275,** H1635-1642.

Lemay M, de Lange E & Kucera JP (2011). Effects of stochastic channel gating and distribution on the cardiac action potential. *J Theor Biol* **281,** 84-96.

Lemay M, de Lange E & Kucera JP (2012). Uncovering the dynamics of cardiac systems using stochastic pacing and frequency domain analyses. *PLoS Comput Biol* **8,** e1002399.

Li M & Otani NF (2003). Ion channel basis for alternans and memory in cardiac myocytes. *Ann Biomed Eng* **31,** 1213-1230.

Ljung L (1999). System Identification - Theory for the User. Prentice Hall, Upper Saddle River, NJ.

Madhvani RV, Xie Y, Pantazis A, Garfinkel A, Qu Z, Weiss JN & Olcese R (2011). Shaping a new Ca^{2+} conductance to suppress early afterdepolarizations in cardiac myocytes. *J Physiol* **589,** 6081-6092.

Mahajan A, Shiferaw Y, Sato D, Baher A, Olcese R, Xie LH, Yang MJ, Chen PS, Restrepo JG, Karma A, Garfinkel A, Qu Z & Weiss JN (2008). A rabbit ventricular action potential model replicating cardiac dynamics at rapid heart rates. *Biophys J* **94,** 392-410.

Milescu LS, Akk G & Sachs F (2005). Maximum likelihood estimation of ion channel kinetics from macroscopic currents. *Biophys J* **88,** 2494-2515.

Mironov S, Jalife J & Tolkacheva EG (2008). Role of conduction velocity restitution and short-term memory in the development of action potential duration alternans in isolated rabbit hearts. *Circulation* **118,** 17-25.

Nolasco JB & Dahlen RW (1968). A graphic method for the study of alternation in cardiac action potentials. *J Appl Physiol* **25,** 191-196.

O'Hara T, Virág L, Varró A & Rudy Y (2011). Simulation of the undiseased human cardiac ventricular action potential: model formulation and experimental validation. *PLoS Comput Biol* **7,** e1002061.

Osadchii OE, Larsen AP & Olesen SP (2010). Predictive value of electrical restitution in hypokalemia-induced ventricular arrhythmogenicity. *Am J Physiol Heart Circ Physiol* **298,** H210-220.

Otani NF, Li M & Gilmour RF, Jr. (2005). What can nonlinear dynamics teach us about the development of ventricular tachycardia/ventricular fibrillation? *Heart Rhythm* **2,** 1261-1263.

Pastore JM, Girouard SD, Laurita KR, Akar FG & Rosenbaum DS (1999). Mechanism linking T-wave alternans to the genesis of cardiac fibrillation. *Circulation* **99,** 1385-1394.

Petrie A & Zhao X (2012). Estimating eigenvalues of dynamical systems from time series with applications to predicting cardiac alternans. *Proc R Soc A* **468,** 3649-3666.

Qu Z, Xie Y, Garfinkel A & Weiss JN (2010). T-wave alternans and arrhythmogenesis in cardiac diseases. *Front Physiol* **1,** 154.

Sato D, Shiferaw Y, Garfinkel A, Weiss JN, Qu Z & Karma A (2006). Spatially discordant alternans in cardiac tissue: role of calcium cycling. *Circ Res* **99,** 520-527.

Taggart P, Orini M, Hanson B, Hayward M, Clayton R, Dobrzynski H, Yanni J, Boyett M & Lambiase PD (2014). Developing a novel comprehensive framework for the investigation of cellular and whole heart electrophysiology in the in situ human heart: historical perspectives, current progress and future prospects. *Prog Biophys Mol Biol* **115,** 252-260.

Tolkacheva EG, Anumonwo JM & Jalife J (2006). Action potential duration restitution portraits of mammalian ventricular myocytes: role of calcium current. *Biophys J* **91,** 2735-2745.

Verrier RL & Malik M (2015). Quantitative T-wave alternans analysis for guiding medical therapy: an underexploited opportunity. *Trends Cardiovasc Med* **25,** 201-213.

Wagner S, Maier LS & Bers DM (2015). Role of sodium and calcium dysregulation in tachyarrhythmias in sudden cardiac death. *Circ Res* **116,** 1956-1970.

Watanabe MA, Fenton FH, Evans SJ, Hastings HM & Karma A (2001). Mechanisms for discordant alternans. *J Cardiovasc Electrophysiol* **12,** 196-206.

Weiss JN, Karma A, Shiferaw Y, Chen PS, Garfinkel A & Qu Z (2006). From pulsus to pulseless: the saga of cardiac alternans. *Circ Res* **98,** 1244-1253.

Wu R & Patwardhan A (2006). Mechanism of repolarization alternans has restitution of action potential duration dependent and independent components. *J Cardiovasc Electrophysiol* **17,** 87-93.

Zaniboni M, Pollard AE, Yang L & Spitzer KW (2000). Beat-to-beat repolarization variability in ventricular myocytes and its suppression by electrical coupling. *Am J Physiol Heart Circ Physiol* **278,** H677-H687.

Additional information

Competing interests

The authors have no competing interests to disclose.

Author contributions

Patch clamp experiments were conducted at the Dept. of Anesthesiology and Perioperative Medicine, Division of Molecular Medicine, University of California, Los Angeles. Computer simulations were conducted at the Department of Physiology, University of Bern.

J.P.K. and E.D.L. conceived and designed the study. R.V.M., M.A., N.P.B., R.O. and Y.P. acquired the data. Y.P. and J.P.K. analysed the data. J.P.K. and Y.P. drafted the manuscript. All authors contributed to the interpretation of the data and to a critical review of the manuscript for important intellectual content.

All authors approved the final version of the manuscript, agree to be accountable for all aspects of the work in ensuring that questions related to the accuracy or integrity of any part of the work are appropriately investigated and resolved and all persons designated as authors qualify for authorship, and all those who qualify for authorship are listed.

Funding

This work was supported by the Swiss National Science Foundation (grant number 31003A-135016/1 to J.P.K.) and the National Heart, Lung and Blood Institute at the National Institutes of Health (grant number P01HL078931 to J.N.W.).

Acknowledgments

We are greatly indebted to Thao Nguyen for her support during experiments.

Translational perspective

The alternation (alternans) of cardiac action potential duration is an intricate dynamical phenomenon leading to life-threatening heart rhythm disorders. Alternans can result from instabilities in ion current dynamics (voltage-driven alternans) or in intracellular calcium cycling (calcium-driven alternans). We examined the susceptibility to alternans of rabbit ventricular myocytes using pacing protocols comprising stochastic (random) beat-to-beat variations of pacing cycle length and tested the hypothesis that such an approach can provide more information about the dynamics of alternans compared to a pacing protocol without variations. From the series of resulting action potential durations, we derived novel markers that not only signal the imminence of alternans, but also discriminate between voltage-driven and calcium-driven alternans. We demonstrated that our approach can identify the change from calcium-driven to voltage-driven alternans dynamics induced by blocking the calcium-induced calcium release from the sarcoplasmic reticulum. Our findings lead to the prospect of implementing stochastic pacing protocols for diagnostic purposes, e.g. in patients undergoing cardiac catheterization investigations or having an implanted pacemaker or defibrillator. This approach may assist to determine the patients' susceptibility to alternans and associated arrhythmias and to identify to what type of alternans the patients are predisposed. Making this distinction is relevant for pharmacotherapy, because the propensity to calcium-driven vs. voltage-driven alternans may require different preventive or therapeutic measures (e.g., drugs acting on potassium currents vs. calcium fluxes) and be associated with different contraindications for certain drugs. Thus, the potential of stochastic pacing deserves further investigations and opens prospects for future basic and translational research.

[Paragraph length: 249 words]

Figures and legends

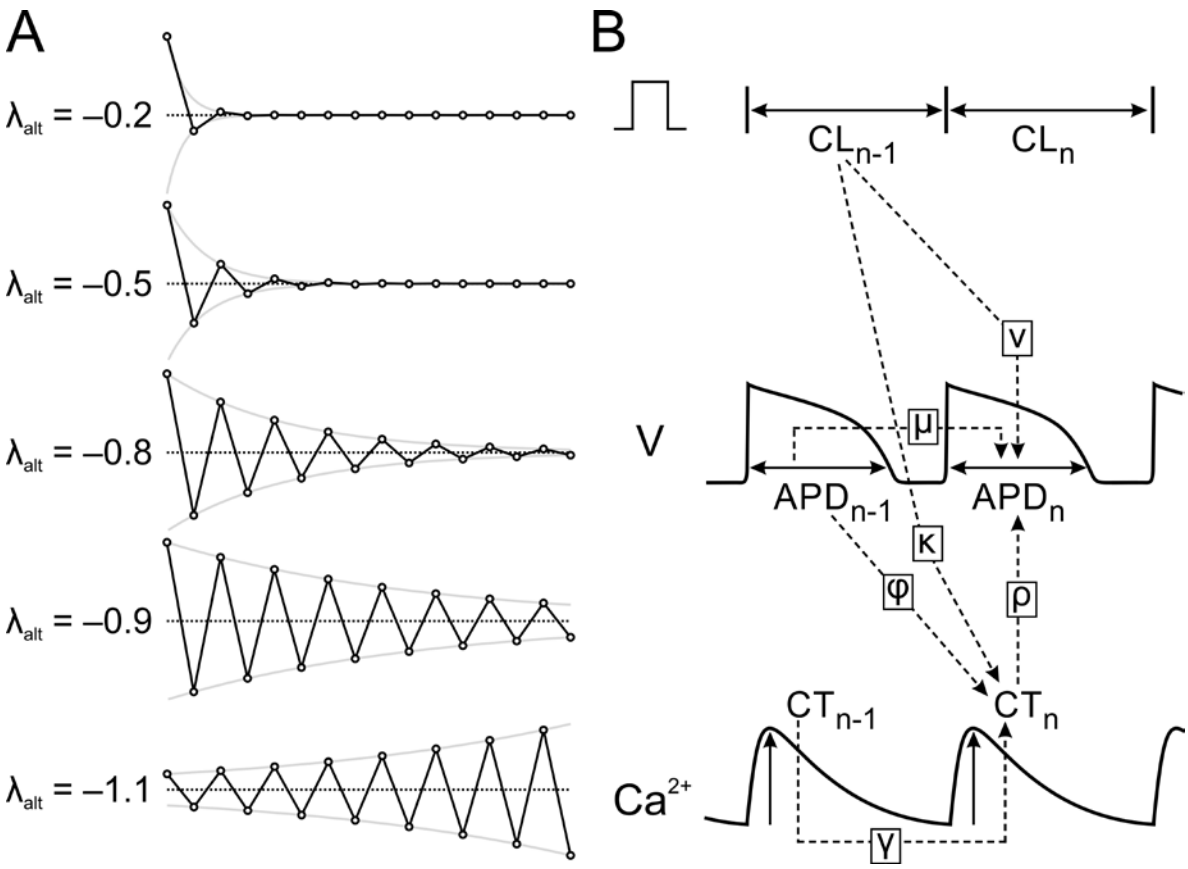

Figure 1. Signification of λ_{alt} and bidirectional interactions between the AP and the Ca^{2+} transient

A, the eigenvalue λ_{alt} represents the factor by which an alternating perturbation decays with every beat. For λ_{alt} close to 0, the alternating eigenmode dissipates rapidly and will not be manifest in a real system subject to continuous perturbations. With λ_{alt} getting closer to –1, alternating sequences are more likely to appear and to endure because the alternans eigenmode dissipates slower. The susceptibility to alternate becomes apparent for λ_{alt} around –0.5 and is quite manifest for $\lambda_{alt} < -0.8$. If $\lambda_{alt} < -1$, the system is unstable and the smallest perturbation is amplified. *B*, theoretical model of the interactions between CL, APD and the Ca^{2+} transient (CT). The interactions (details in the text) are marked with dotted arrows labelled with Greek letters.

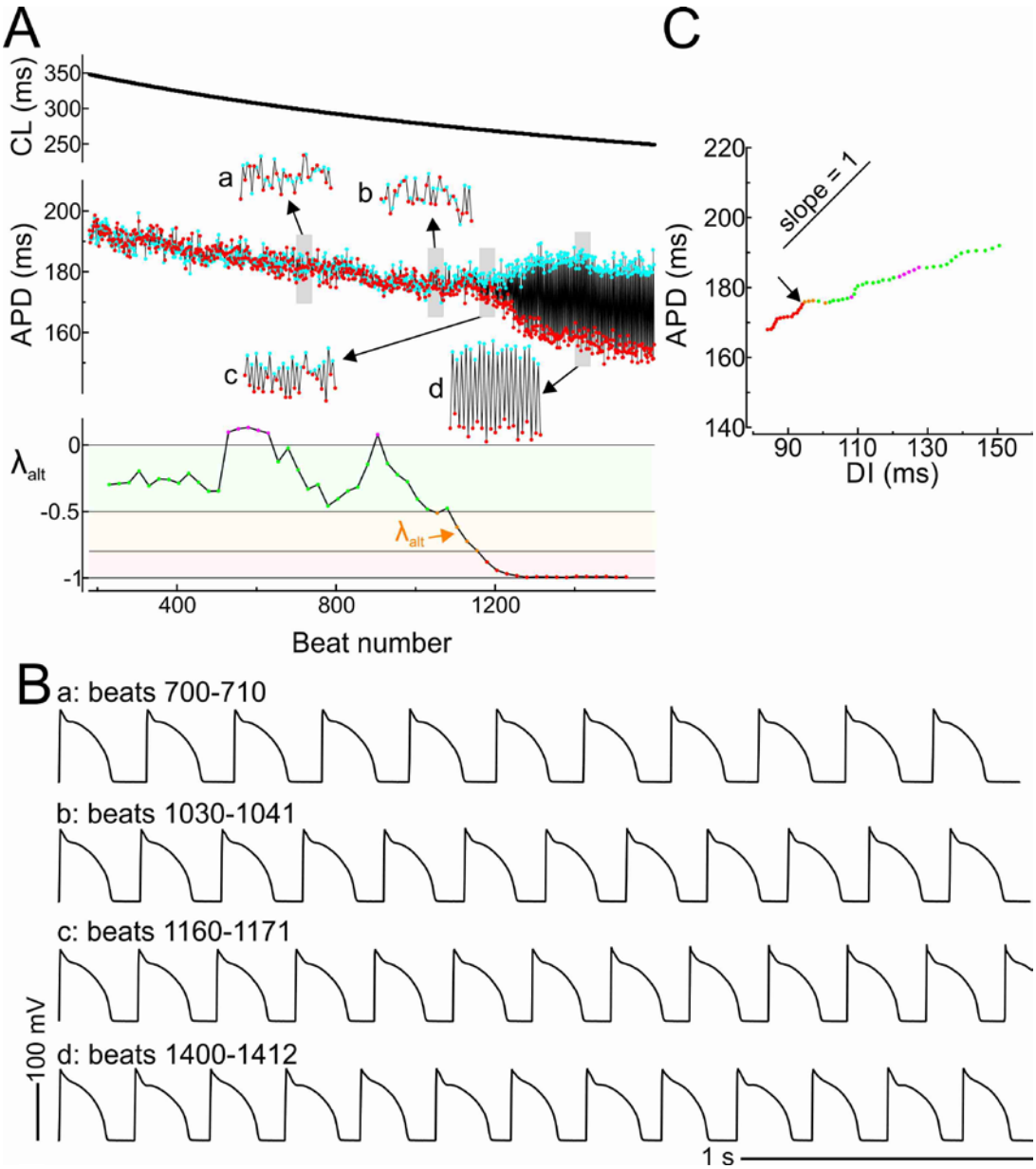

Figure 2. Ramp protocol without stochastic variations in a ventricular myocyte

A, pacing CL, APD and λ_{alt} (sliding window of 100 beats) vs. beat number. Odd and even APDs are shown in red and cyan, respectively. λ_{alt} is shown with distinct background colours (green: $0>\lambda_{alt}>-0.5$; orange: $-0.5\geq\lambda_{alt}>-0.8$; red: $\lambda_{alt}<-0.8$). Data points in magenta indicate that λ_{alt} was complex (the real part is shown). *B*, APs corresponding to the first 11-13 beats of the insets labelled a-d in *A*. *C*, plot of mean APD vs. mean DI in the sliding window, using the colour defined above for λ_{alt}. The onset of sustained alternans is denoted by the arrow.

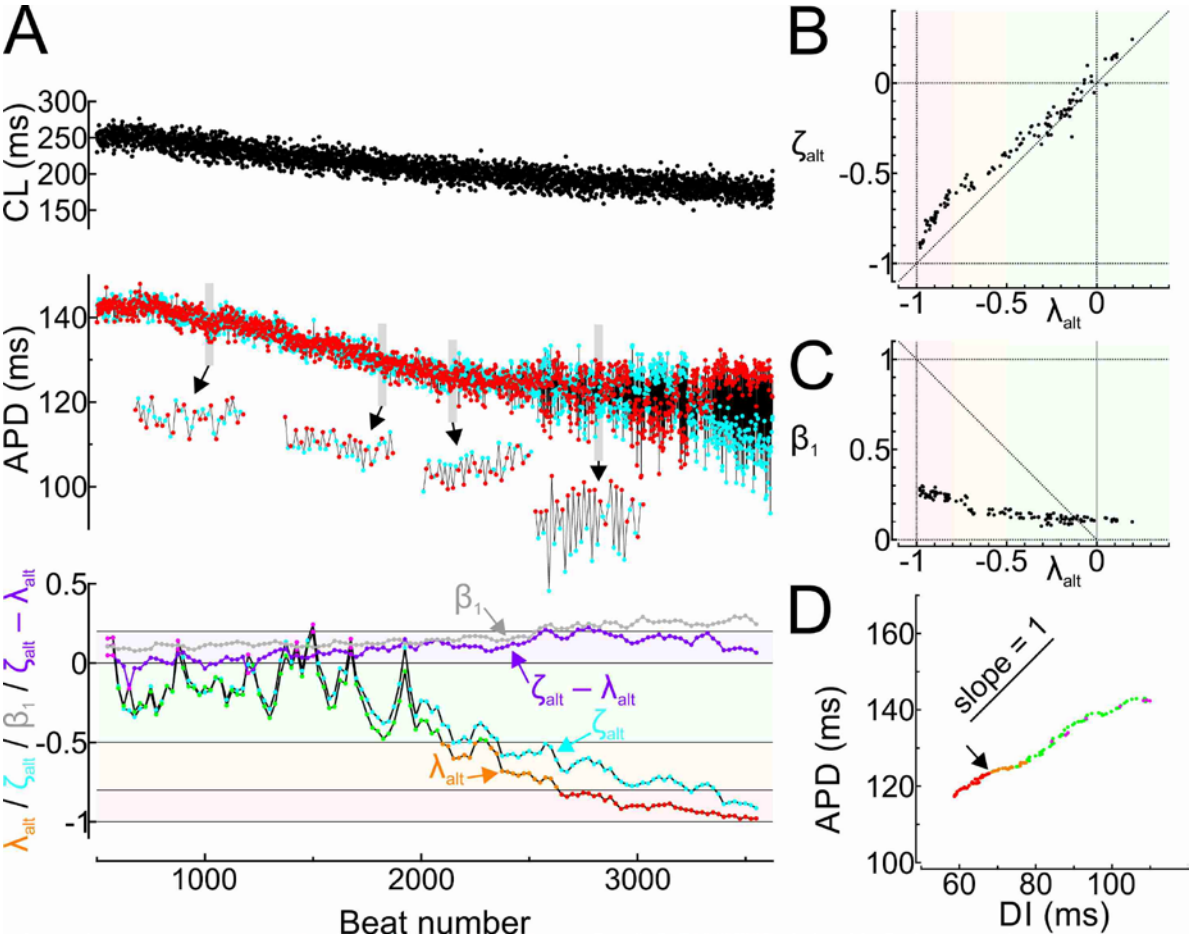

Figure 3. Ramp protocol with stochastic variations in a ventricular myocyte

A, pacing CL, APD, λ_{alt}, ζ_{alt} (cyan), β_1 (S1S2 restitution slope, grey) and difference ζ_{alt}–λ_{alt} (purple) vs. beat number, computed in the sliding window. Odd and even APDs are shown in red and cyan, respectively. λ_{alt} is shown with distinct background colours, as in Fig. 2. Data points in magenta indicate that λ_{alt} was complex (the real part is shown). *B*, plot of ζ_{alt} vs. λ_{alt} during the experiment. *C*, plot of β_1 vs. λ_{alt} during the experiment. *D*, plot of mean APD vs. mean DI in the sliding window, using the colour defined in *A* for λ_{alt}. The onset of full alternans is denoted by the arrow.

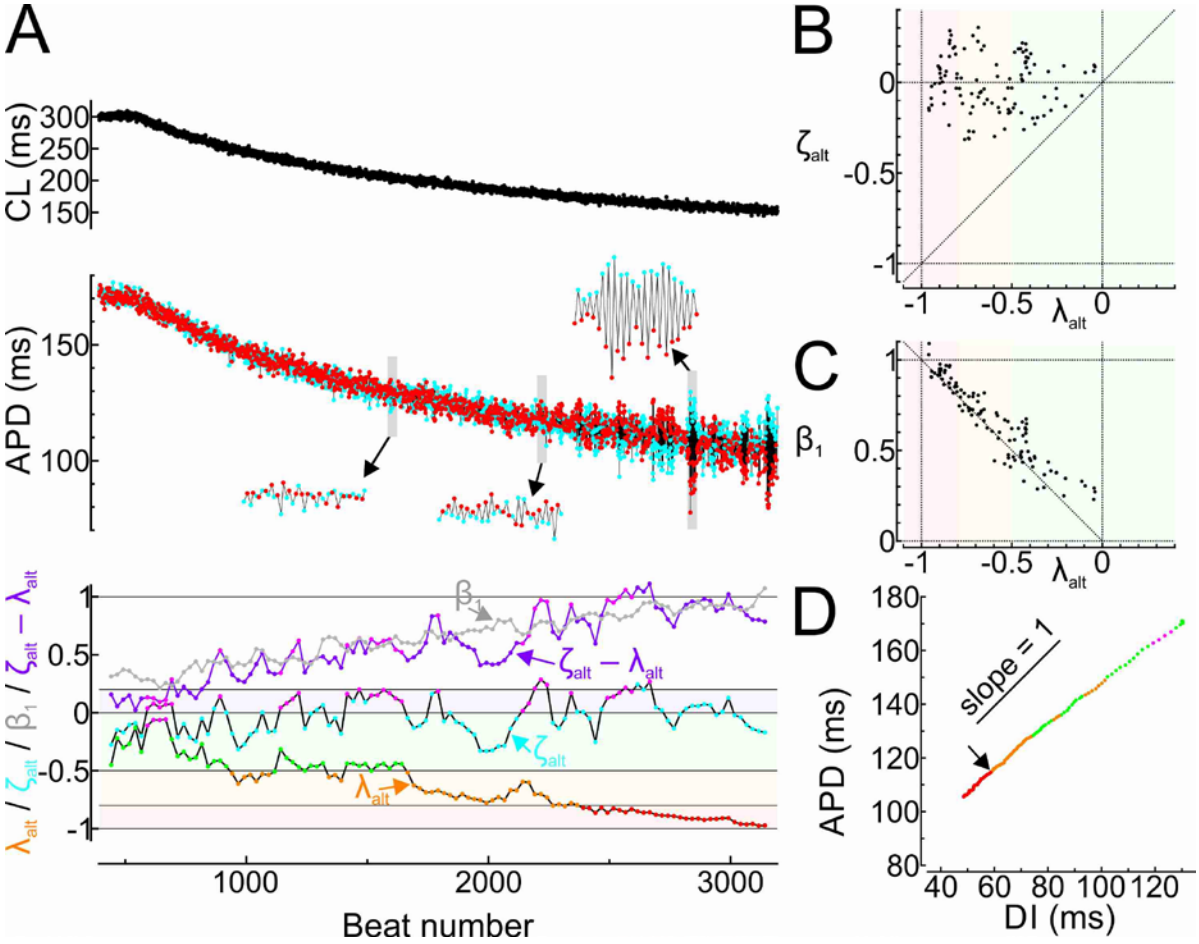

Figure 4. Ramp protocol with stochastic variations in a ventricular myocyte exposed to 100 µmol/L ryanodine

Same layout as in Figure 3.

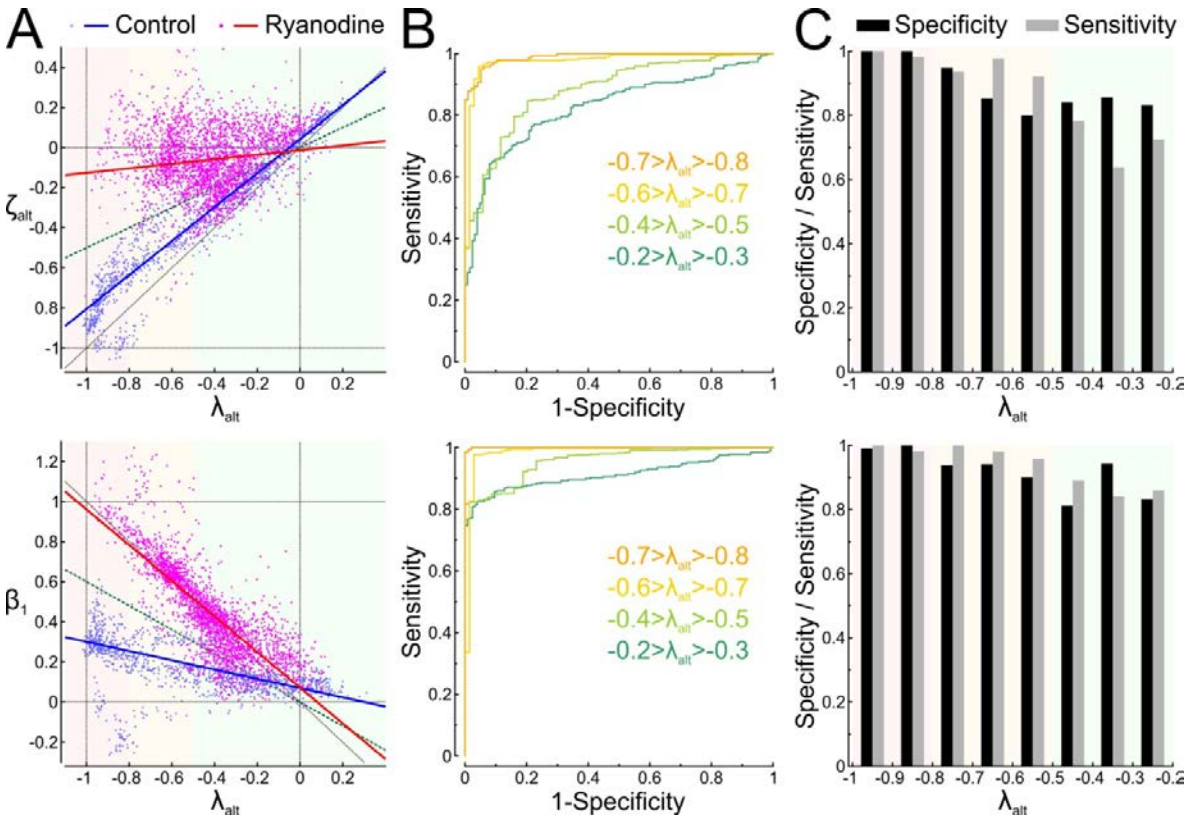

Figure 5. Discriminative capability of ζ_{alt} and β_1

A, plot of ζ_{alt} (top) and β_1 (bottom) vs. λ_{alt} for all experiments pooled together (blue: control without ryanodine (10 cells from 6 animals); magenta: 100 µmol/L ryanodine (15 cells from 9 animals)). Blue and red lines are corresponding regression lines. *B*, receiver operating characteristic curves for ζ_{alt} (top) and β_1 (bottom) for data in different bins of λ_{alt}. *C*, specificity and sensitivity of the criteria $\zeta_{alt}>0.5\cdot\lambda_{alt}$ (top) and $\beta_1>-0.6\cdot\lambda_{alt}$ (bottom) to detect the use of ryanodine (these criteria are shown as green dotted lines in *A*).

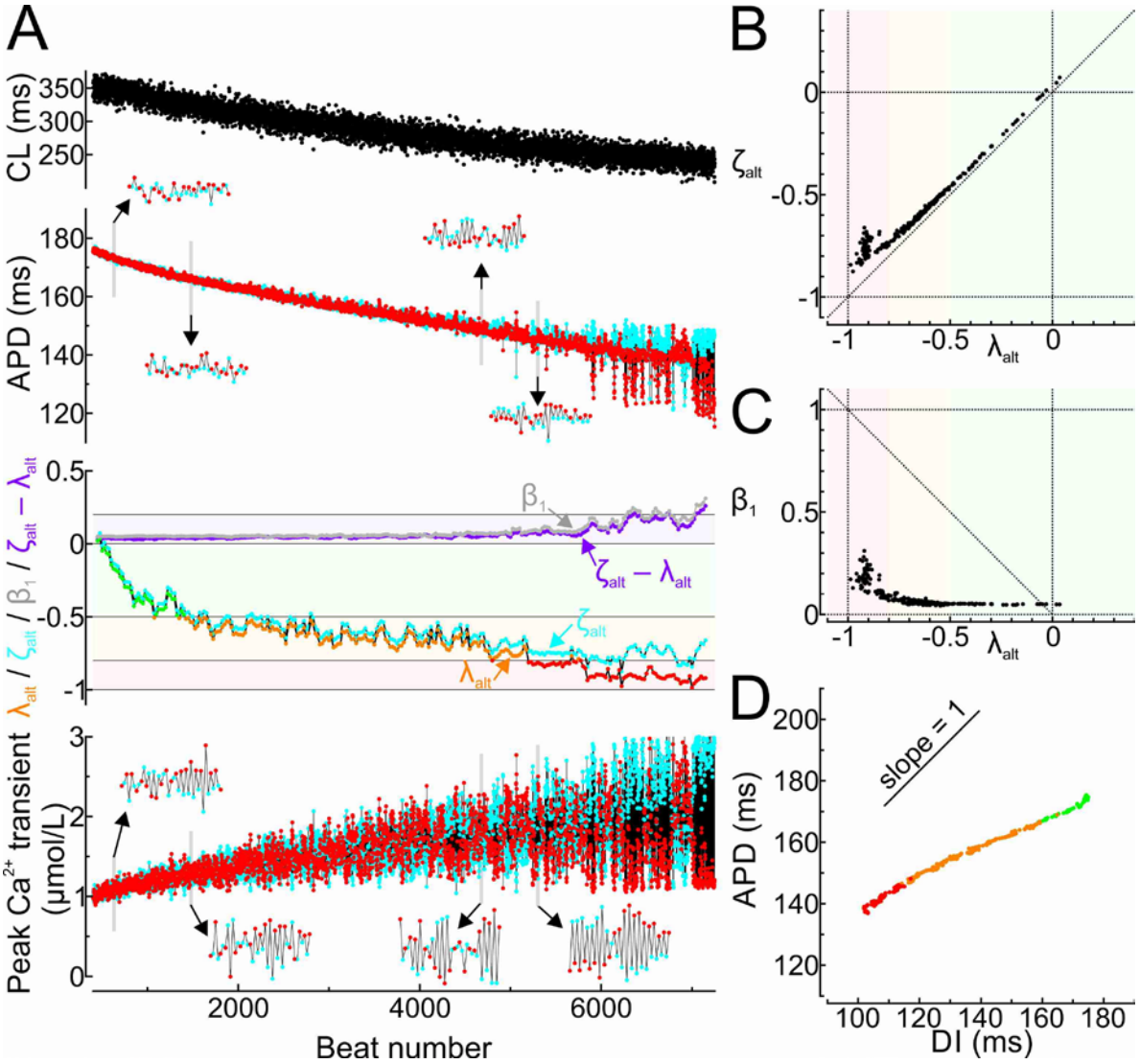

Figure 6. Ramp protocol with stochastic variations in the Mahajan *et al*. model

A, pacing CL, APD, λ_{alt}, ζ_{alt} (cyan), β_1 (S1S2 restitution slope, grey), difference $\zeta_{alt} - \lambda_{alt}$ (purple) computed in a sliding window (100 beats), and peaks of the Ca^{2+} transients. Odd and even APDs and corresponding Ca^{2+} transient peaks are shown in red and cyan, respectively. λ_{alt} is shown in distinct bands using different colours (green: $0 > \lambda_{alt} > -0.5$; orange: $-0.5 \geq \lambda_{alt} > -0.8$; red: $\lambda_{alt} < -0.8$). *B*, plot of ζ_{alt} vs. λ_{alt} during the simulation. *C*, Plot of β_1 vs. λ_{alt} during the simulation. *D*, plot of mean APD vs. mean DI in the sliding window, using the colour defined above for λ_{alt}.

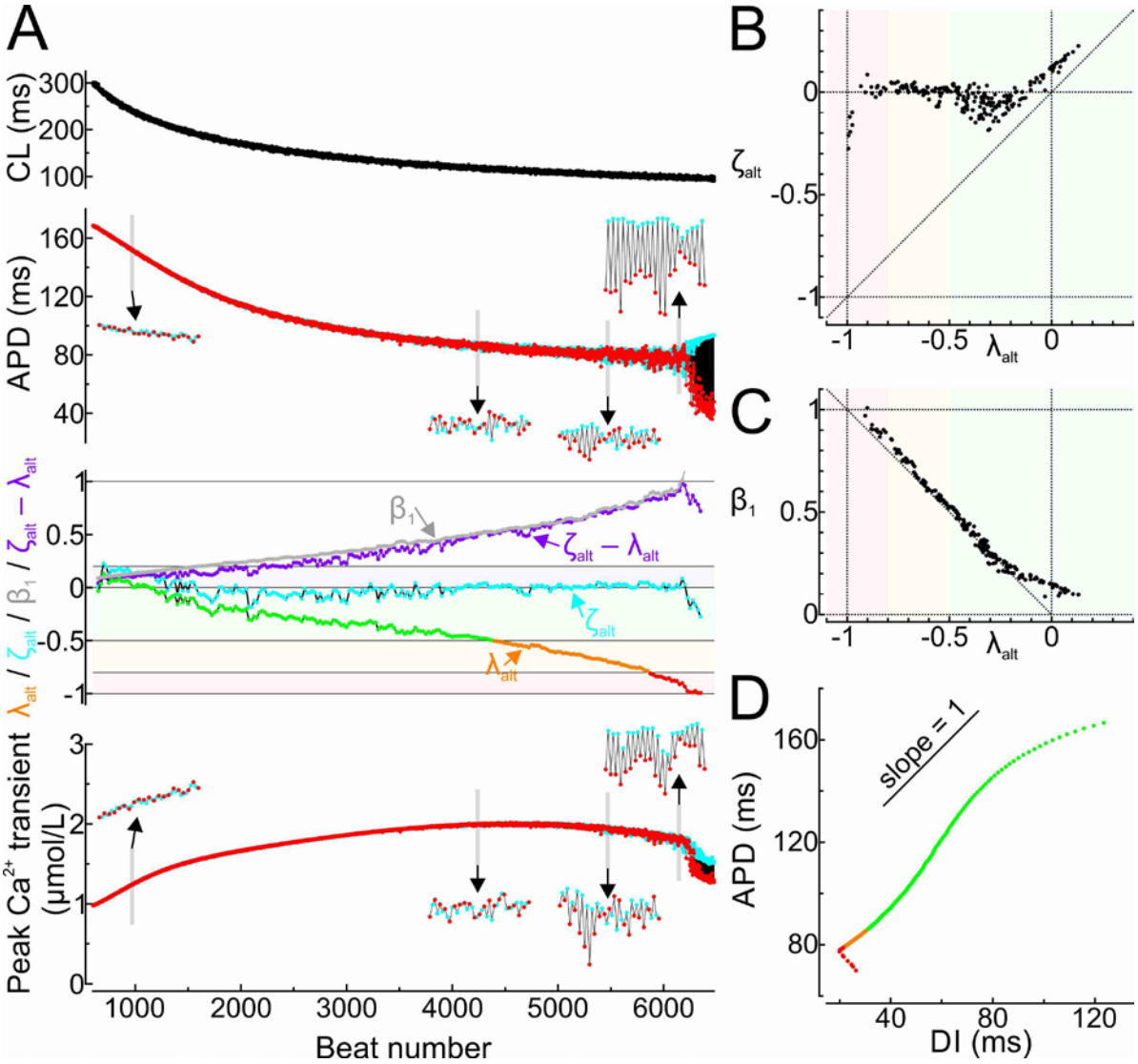

Figure 7. Ramp protocol with stochastic variations in the Mahajan *et al*. model with Ca^{2+} release strength reduced by 90%

Same layout as in Figure 6.

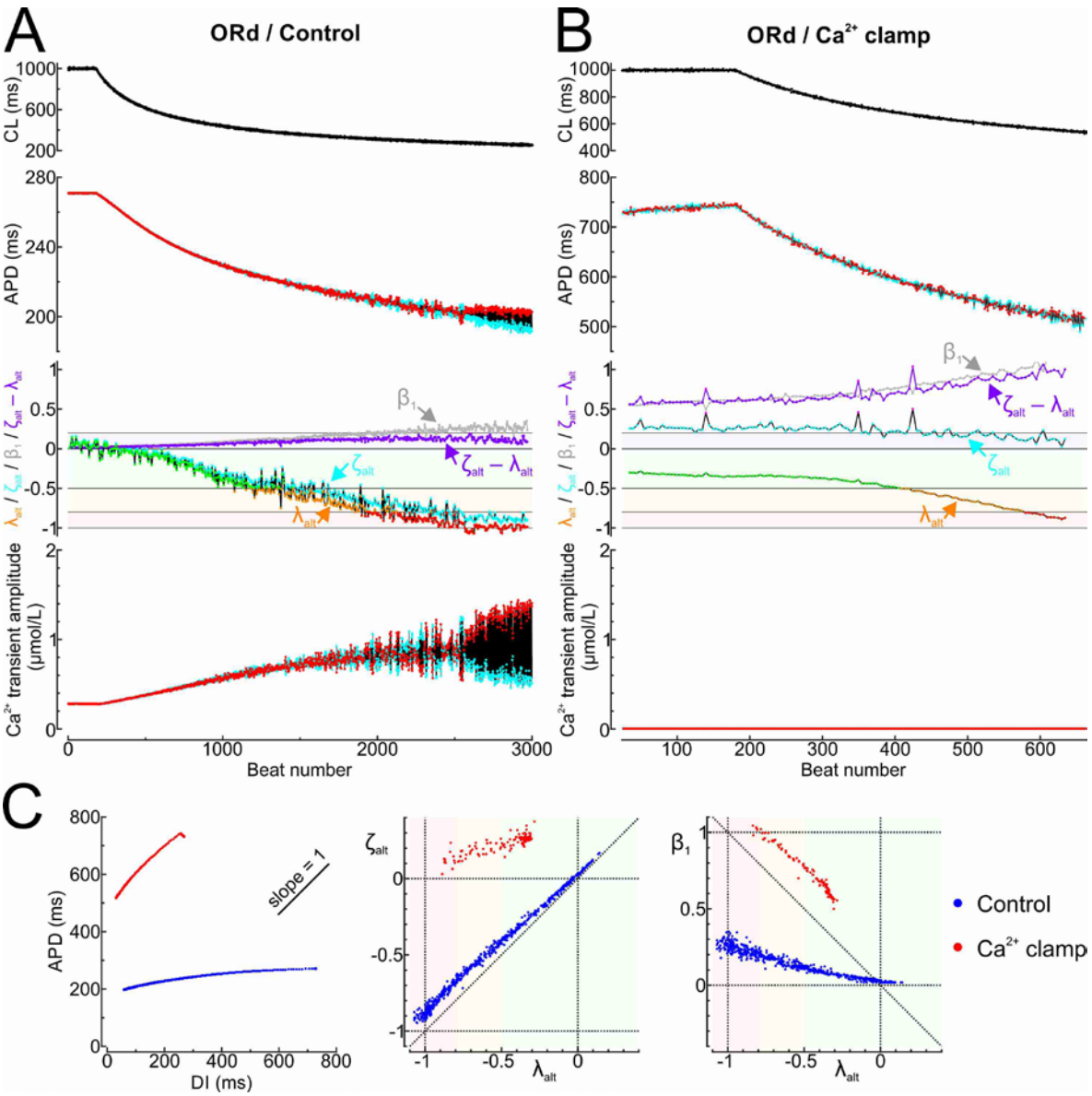

Figure 8. Ramp protocol with stochastic variations in the ORd human ventricular cell model under control conditions and under conditions of Ca^{2+} clamp

A, control ORd model. Pacing CL, APD, markers λ_{alt}, ζ_{alt}, β_1 and ζ_{alt}–λ_{alt} (sliding window of 16 beats) as well as Ca^{2+} transient amplitude are shown vs. beat number. Layout similar to Figures 6*A* and 7*A*. *B*, ORd model with all Ca^{2+} concentrations clamped to their initial values. Same layout as in *A*. *C*, superimposed plots of mean APD vs. mean DI (left) in the sliding window, ζ_{alt} vs. λ_{alt} (middle), and β_1 vs. λ_{alt}. (right) for the two situations investigated in *A* and *B*.